Berardinelli-Seip congenital lipodystrophy 2 regulates adipocyte lipolysis, browning, and energy balance in adult animals[S]

Hongyi Zhou,* Xinnuo Lei,* Tyler Benson,† James Mintz,† Xiaojing Xu,§ Ruth B. Harris,* Neal L. Weintraub,† Xiaoling Wang,§ and Weiqin Chen[1,*]

Department of Physiology,* Vascular Biology Center,† Georgia Prevention Institute, Department of Pediatrics,§ Georgia Regents University, Augusta, GA 30912

Abstract **Mutations in *BSCL2/SEIPIN* cause Berardinelli-Seip congenital lipodystrophy type 2 (BSCL2), but the mechanisms whereby Bscl2 regulates adipose tissue function are unclear. Here, we generated adipose tissue (mature) Bscl2 knockout (Ad-mKO) mice, in which Bscl2 was specifically ablated in adipocytes of adult animals, to investigate the impact of acquired Bscl2 deletion on adipose tissue function and energy balance. Ad-mKO mice displayed reduced adiposity and were protected against high fat diet-induced obesity, but not insulin resistance or hepatic steatosis. Gene expression profiling and biochemical assays revealed increased lipolysis and fatty acid oxidation in white adipose tissue (WAT) and brown adipose tissue , as well as browning of WAT, owing to induction of cAMP/protein kinase A signaling upon Bscl2 deletion. Interestingly, Bscl2 deletion reduced food intake and downregulated adipose β3-adrenergic receptor (ADRB3) expression. Impaired ADRB3 signaling partially offsets upregulated browning-induced energy expenditure and thermogenesis in Ad-mKO mice housed at ambient temperature. However, this counter-regulatory response was abrogated under thermoneutral conditions, resulting in even greater body mass loss in Ad-mKO mice.** **These findings suggest that Bscl2 regulates adipocyte lipolysis and β-adrenergic signaling to produce complex effects on adipose tissues and whole-body energy balance.**—Zhou, H., X. Lei, T. Benson, J. Mintz, X. Xu, R. B. Harris, N. L. Weintraub, X. Wang, and W. Chen. **Berardinelli-Seip congenital lipodystrophy 2 regulates adipocyte lipolysis, browning, and energy balance in adult animals.** ***J. Lipid Res.*** **2015.** 56: **1912–1925.**

Supplementary key words adipose tissue • lipolysis and fatty acid metabolism • triglycerides • obesity • beta-oxidation

Berardinelli-Seip congenital lipodystrophy (BSCL) is an autosomal recessive disorder characterized by a near total absence of body fat from birth or infancy and associated with severe metabolic abnormalities including hyperinsulinemia, hypertriglyceridemia, insulin resistance, and type 2 diabetes (1–3). To date, mutations involving four different genes, *BSCL1*, *BSCL2*, *CAV1*, and *PTRF*, have been linked to this rare genetic disorder, with the first two accounting for about 95% of reported cases (4–7). BSCL type 2 (BSCL2), caused by mutations in *BSCL2* (also known as *SEIPIN*), is the most severe form of BSCL (7). BSCL2 is an integral endoplasmic reticulum (ER) membrane protein expressed in most tissues, including testes and neuronal and adipose tissues (7–9). Global embryonic deletion of Bscl2 in mice leads to lipodystrophy, insulin resistance, fatty liver, and organomegaly, recapitulating human BSCL2 (10–12). Bscl2 knockout rats also demonstrated a lipodystrophic phenotype in addition to impairment in brain development and spermatogenesis (13). Various mechanisms whereby Bscl2 regulates adipose tissue function have been proposed in different species, including regulation of lipid droplet (LD) biogenesis in yeast (14–17), sarcoendoplasmic reticulum calcium transport in *Drosophila* (18), and phospholipid metabolism and PPARγ activity in rodents (19). Human Bscl2 was also reported to interact in vitro with two enzymes of the

This work was supported by the American Heart Association Scientist Development Grant 12SDG9080000 and Georgia Regents University start-up funds to W.C. and by National Heart, Lung and Blood Institute grant HL112640 to N.L.W. The RNA-sequencing project was supported by the Illumina Georgia Regents University Cancer Center RNA-Seq grant. The authors declare no conflicts of interest.

Manuscript received 27 April 2015 and in revised form 10 August 2015.

Published, JLR Papers in Press, August 12, 2015
DOI 10.1194/jlr.M060244

Abbreviations: Ad-mKO, adipose tissue (mature) type 2 Berardinelli-Seip congenital lipodystrophy knockout; ADRB3, β3-adrenergic receptor; AGPAT2, 1-acylglycerol-3-phosphate O-acyltransferase 2; AR, adrenergic receptor; ASKO, adipose-specific SEIPIN knockout; BAT, brown adipose tissue; BSCL, Berardinelli-Seip congenital lipodystrophy; BSCL2, Berardinelli-Seip congenital lipodystrophy type 2; CD, chow diet; Ctrl, control; ER, endoplasmic reticulum; eWAT, epididymal white adipose tissue; GO, gene ontology; H&E, hematoxylin and eosin; HFD, high fat diet; KRBH, Krebs-Ringer bicarbonate-HEPES; LD, lipid droplet; LPA: lysophosphatidic acid; NE, norepinephrine; PA, phosphatidic acid; PKA, protein kinase A; RER, respiratory exchange ratio; RNA-seq, RNA-sequencing; sWAT, subcutaneous white adipose tissue; TAM, tamoxifen; WAT, white adipose tissue.

[1]To whom correspondence should be addressed.
e-mail: wechen@gru.edu

[S] The online version of this article (available at http://www.jlr.org) contains a supplement.

TG synthesis pathway, 1-acylglycerol-3-phosphate O-acyltransferase 2 (AGPAT2) and phosphatidate phosphatase (LPIN1) (20, 21). However, whether these or other pathways are directly responsible for the failure of adipogenesis in mammalian Bscl2-deficient cells remains to be determined.

The promotion of brown fat properties in white adipose tissue (WAT) (i.e., browning) has been proposed as a promising approach to treating obesity and its complications (22–24). Activation of the sympathetic nervous system through β-adrenergic receptors (ARs), in particular β3-AR (ADRB3), which is predominantly expressed in adipose tissue (25), is closely linked to the induction of thermogenic beige adipocytes (also known as brite, inducible brown, or brown-like adipocytes) in rodents and humans (26–29). Cold exposure or ADRB3 agonists activate the classic lipolytic pathway through ARs to stimulate cAMP/protein kinase A (PKA) signaling, lipid mobilization, and browning in WAT (30). Bscl2-deficient murine embryonic fibroblasts or stromal vascular cells exhibited increased basal cAMP/PKA-mediated lipolysis during differentiation, leading to termination of adipogenesis (10, 12). Conversely, adipose-specific SEIPIN knockout (ASKO) mice with FABP4-Cre-mediated Bscl2 deletion exhibited decreased lipolysis in response to β-AR agonists in vivo (19). The reasons for these apparently discrepant findings are unclear. Moreover, whether Bscl2 influences browning of mature WAT to regulate adiposity and energy balance, independent of its effect on adipocyte differentiation and adipose tissue development, is unknown.

In this study, we utilized the tamoxifen (TAM)-inducible adiponectin promoter driven Cre^{ERT2}-LoxP system to generate adipose tissue (mature) Bscl2 knockout (Ad-mKO) mice, in which Bscl2 is specifically deleted in mature adipocytes of adult animals, to investigate the impact of acquired Bscl2 deficiency. Our findings identify Bscl2 as a regulator of lipolysis, browning, and ADRB3 signaling in mature adipocytes, suggesting that Bscl2 is not only essential for adipocyte differentiation and adipose tissue development, but that it also regulates the function of mature adipocytes with regard to whole-body energy balance.

MATERIALS AND METHODS

Mice

Bscl2$^{f/f}$ mice (10) were backcrossed to C57BL/6 for eight generations and then interbred with mice in which Cre expression is driven by adiponectin promoter-induced by TAM [*AdipqCre*$^{ERT2+}$ mice (31)] to generate TAM-inducible Ad-mKO mice. Male mice (8–10 weeks old) were gavaged with TAM (Sigma, St. Louis, MO) for five consecutive days at 4 mg/20 g of body weight. All studies used *Bscl2*$^{f/f}$ littermates simultaneously treated with TAM as wild-type control (Ctrl) mice (Fig. 1A). All mice, unless specified, were maintained under standard conditions with controlled 12 h light-dark cycle at 21°C ambient temperature. Mice were fed with a chow diet (CD) (2018 Teklad Global 18% protein rodent diet; Harlan Laboratories). For diet-induced obesity, 12 days after TAM treatment, mice were fed a high fat diet (HFD) (60% fat by kcal, D12492; Research Diets Inc.) until the end of the experimental protocol. Body weight was measured weekly. All animal experiments were approved by the IACUC at Georgia Regents University (IACUC file #2012-0462).

Histology and adipocyte size determination

Tissue samples were fixed, processed, and stained with hematoxylin and eosin (H&E). Adipocyte size was analyzed with Image J software.

Immunohistochemistry and immunofluorescent staining

For UCP1 immunohistochemistry, paraffin-embedded sections were incubated with anti-UCP1 (ab10983; Abcam), followed by detection using the ABC Vectastain Elite kit (Vector Labs) according to the manufacturer's instructions. For PLIN1 immunofluorescent staining, paraffin-embedded sections were incubated with anti-PLIN1 (GP29; Progen) followed by detection using Texas red goat anti-guinea pig IgG conjugate (Vector Labs).

Systemic tests

Insulin tolerance tests were performed in mice fasted for 6 h and then injected ip with human insulin (Humulin; Novo Nordisk) at 0.75 U/kg for mice on CD, and 2.0 U/kg for mice on HFD. Glucose tolerance tests were performed in mice fasted for 6 h and then injected ip (for mice on CD) or administered by gastric gavage (for mice on HFD) with glucose (1.5 g/kg body weight). Blood glucose levels were measured by One-touch Ultra glucose meter before and at 15, 30, 60, and 120 min after glucose administration. Insulin and leptin levels were measured using commercial ELISA kits (Millipore). Glycerol and NEFA levels were determined using a free glycerol reagent (Sigma-Aldrich) and WAKO NEFA analysis kit (NEFA-HR(2); Wako Pure Chemical Industries), respectively. Tissue TGs were extracted according to Bligh and Dyer (32), and dissolved in chloroform. A small aliquot (5–30 μl) was removed and dried. The TG concentration in this aliquot was determined using a TG assay kit (Thermo DMA) and normalized to tissue weight (33).

Body composition and analysis of energy balance

Fat and lean body masses were measured by NMR-based Bruker Minispec mq10 in mice fed CD (performed by Vanderbilt Mouse Metabolic Phenotyping Center). Activity, food consumption, oxygen consumption, and energy expenditure for mice, 3 weeks after TAM administration, were assessed in a metabolic monitoring system [Comprehensive Lab Animal Monitoring System (CLAMS); Columbus Instruments, Columbus, OH] for 4 days (2 days of acclimation followed by 2 days of measurement) according to the manufacturer's protocols. Indirect calorimetry analyses with mice 12 weeks after TAM administration were performed by Vanderbilt Mouse Metabolic Phenotyping Center following their standard protocol, using a computer-controlled indirect calorimetry system (Promethion; Sable Systems, Las Vegas, NV). All measurements were expressed as per mouse or normalized to body weight. Locomotor activity was measured by counting the number of infrared beam breaks on x and z axes during the measurement period. Energy expenditure in response to norepinephrine (NE) was measured in Ctrl and Ad-mKO mice 12 weeks after TAM administration, following completion of the basal readings in the original metabolic cages (Vanderbilt Mouse Metabolic Phenotyping Center). The mice were removed from the metabolic chambers for a short time (6 min) and injected subcutaneously with NE (A7257; Sigma) at 1 mg/kg before returning to the metabolic chambers where O_2 consumption and CO_2 production were recorded continuously for another 60 min, as previously described (34). Experiments were carried out at ambient temperature (21°C). Cold acclimation was tested in mice housed individually at 4°C in the presence of food. Rectal body temperatures were measured by a BAT-12 thermometer (Physitemp).

RNA-sequencing and data analysis

RNA was isolated from adipose tissue using Trizol™, and cDNA libraries were generated using the Illumina TruSeq RNA sample preparation kit following the manufacturer's instructions. Briefly, mRNA was isolated by oligo-dT beads and fragmented using divalent cations at 95°C for 5 min. Fragmented mRNA was converted to cDNA that was further purified and subjected to an adaptor ligation containing the respective index sequences. Six samples were pooled onto a single lane for Illumina Hiseq2500 multiplex sequencing under a 50 cycle paired-end protocol. The Illumina sequencing tool, Casava version 1.8, was employed for converting raw images to base calls, generating sequence reads, and demultiplexing the reads into the corresponding index-attached files. The generated FASTQ files were aligned to the mouse genome mm9 by using the TopHat program. The R package, DESeq, was employed for differential expression testing based on the raw counts of sequencing data. Differential testing was performed using negative binomial distribution and size factor-normalized data, and was limited to the genes with overall sum of counts (irrespective of biological condition) >10 [PMID: 20979621]. The differential gene profiles were subsequently produced as indicated, in terms of "log2 fold changes" with P values between the two tested groups. Based on the top 200 genes that showed the most significant differences ($P < 0.05$), enrichment of the gene ontology (GO) biological process terms was analyzed using the GOEAST [PMID: 18487275] program.

Transcriptional profiling by real-time quantitative PCR

Total RNA was isolated from tissues with TRIzol (Invitrogen) and reverse-transcribed using MLV-V reverse transcriptase using random primers (Invitrogen). Real-time quantitative RT-PCR was performed on the Stratagene MX3005. Data were normalized to two housekeeping genes (cyclophilin A and 36B4) based on the geNorm algorithm (https://genorm.cmgg.be/) and expressed as fold changes relative to Ctrl mice. All tissue gene expression studies were performed in mice after a 4 h fast. Supplementary Table 2 lists the RT-PCR primer sequences for genes that were analyzed.

Lipolysis in vitro, ex vivo, and in vivo

Adipocytes from epididymal WAT (eWAT) and brown adipose tissue (BAT) were isolated using collagenase IV digestion (2 mg/ml). After washing, adipocytes (1.5×10^5 cells) were incubated with Krebs-Ringer bicarbonate-HEPES (KRBH) buffer (pH 7.4), supplemented with 2% fatty acid-free BSA and 5.5 mM glucose for 2 h at 37°C with occasional shaking in the absence or presence of 10 μM CL316,243. Cell-free buffer was collected for glycerol and NEFA levels. Data were expressed as glycerol or NEFA released per 1.5×10^5 cells during 2 h incubation. For brown adipocyte lipolysis, data were normalized to total lipid content, as previously described (35). For ex vivo lipolysis, epididymal fat pads were removed postmortem and cut into 10–15 mg pieces. Fat pads (three explants from each animal) were further minced to ~2 mm pieces and distributed into 48-well plates containing 0.25 ml KRBH-2% fatty acid-free BSA medium for 2 h at 37°C in a humidified atmosphere saturated with 95% O_2-5% CO_2 (n = 5 per genotype per experiment). The medium was then collected for determination of glycerol and NEFA levels and normalized to wet tissue weight. For β3-AR-agonist-induced in vivo lipolysis assays, mice were first fasted for 4 h. Blood samples were obtained before and 15 min following ip injection of PBS or 0.1 mg kg^{-1} CL316,243 (Sigma-Aldrich) for determination of NEFA and glycerol levels.

Fatty acid oxidation

Minced fat pads were washed in KRBH plus 2% BSA buffer and placed in 1 ml incubation medium in 13 ml round bottom polystyrene tubes. Fatty acid oxidation was performed ex vivo, as previously described (36). Fatty acid oxidation in isolated adipocytes was performed as previously described with modifications (35). Briefly, adipocytes were isolated by collagenase digestion and washed in KRBH plus 2% BSA and 5.5 mM glucose buffer. Incubation medium was added to suspend the adipocytes at 1.5×10^5 cells/ml. Equal (1 ml) aliquots of cell suspensions were transferred to 13 ml polystyrene tubes and incubated in KRBH medium supplemented with 2% BSA, 5.5 mM glucose, 300 μM palmitic acid and 0.4 μCi/ml [1-^{14}C]palmitic acid (Perkin Elmer Life Sciences). Tubes were then sealed with a rubber stopper which contained hyamine hydroxide-soaked filter paper and incubated at 37°C for 2 h while gently shaking every 30 min. After 2 h, 500 μl 1 M perchloric acid was injected into the tubes to release the [^{14}C]CO_2, and the incubation was continued at 37°C for 1 h. Fatty acid oxidation with BAT homogenates was performed as previously described (37). Pieces of BAT tissue (~15 mg) were placed in STE buffer [1 M sucrose, 10 mM Tris (pH 7.5), and 1 mM EDTA] containing a protease inhibitor and homogenized using a Teflon dounce homogenizer (eight strokes). Tissue homogenates (20 μl) were used to measure fatty acid oxidation for 1 h. The [^{14}C]CO_2 released was measured by scintillation counting of the filter paper, while acid-soluble metabolites were analyzed by centrifugation and counting of ^{14}C radioactivity in the supernatant. Data were normalized to the tissue weight for fat explant and the total protein content for BAT homogenates, respectively.

Immunoblot analysis

Tissues were homogenized and lysed in lysis buffer containing 25 mM Tris-HCl (pH 7.4), 150 mM NaCl, 2 mM EDTA, 1% Triton X-100, and 10% glycerol with freshly added protease inhibitor cocktail (Sigma) and 50 mM NaF, 10 mM sodium pyrophosphate, and 1 mM sodium vanadate. The protein concentration was determined by BCA protein assay (Bio-Rad). Equal amounts of proteins were loaded and immunoblot analysis was carried out according to standard protocol. The following antibodies were used: rabbit polyclonal Bscl2 antisera (directed against C-terminal 17 amino acids of mouse Bscl2; Thermo Scientific); rabbit antibodies against p-AKT-Ser473 (4060), AKT (9272), IRβ (3025), phospho-PKA substrate (9624), HSL (4107S), and phospho-HSL (Ser563) (4139S) (Cell Signaling Technology); GAPDH (Fisher Scientific); PLIN1 (GP29; Progen Biotechnik); ATGL (10006409; Caymen Chemicals); PLIN2 (38); GAPDH (MAB374; Fisher Scientific); ADRB3 (Sc-1473; Santa Cruz); and UCP1 (AB1426; Millipore).

Statistical analysis

Quantitative data are presented as mean ± SEM. Experiments were performed from at least two independent cohorts. Differences between groups were examined for statistical significance with two-tailed Student's t-test or by two-way ANOVA using SigmaPlot software. $P < 0.05$ was considered statistically significant.

RESULTS

Adipose tissue-specific deletion of Bscl2 in adult animals causes progressive fat loss

To examine the cell-autonomous role of Bscl2 in mature adipocytes, we generated Bscl2 Ad-mKO mice (**Fig. 1A**). RT-PCR indicated that 12 days after TAM administration, Bscl2 was selectively deleted in WAT and BAT, but not in

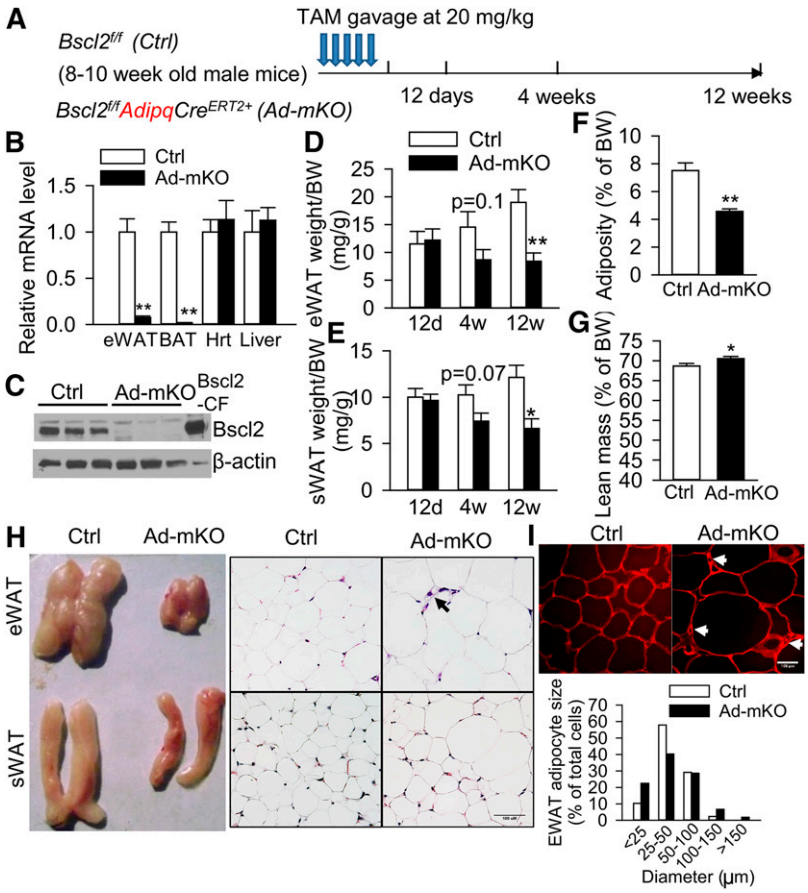

Fig. 1. Acquired loss of Bscl2 in mature adipose tissue reduces adiposity and induces white adipocyte remodeling. A: Strategy in generating TAM-inducible adipose-specific deletion of Bscl2 gene by gavaging TAM daily for five consecutive days in adult 8–10-week-old male *Bscl2*$^{f/f}$ (Ctrl) and *Bscl2*$^{f/f}$ *AdipqCre*$^{ERT2+}$ (Ad-mKO) mice. B, C: Detection of Bscl2 in adipose tissue by RT-PCR (B) and Western blot (C) of eWAT in mice 12 days (12d) after TAM treatment. D: eWAT. E: sWAT mass as normalized to body weight (BW) 12 days, 4 weeks (4w), and 12 weeks (12w) after TAM treatment. Overall fat mass (F) and lean mass (G) as normalized to BW [n = 6–8 per group for (B–G)]. H: Gross anatomy and representative images of H&E-stained sections of eWAT and sWAT from Ctrl and Ad-mKO mice 12 weeks after TAM treatment. Arrow indicates smaller adipocytes. Scale bar = 100 μm. I. Representative confocal images of PLIN1-stained adipose tissue and the average diameter (in microns) of 500 adipocytes in eWAT from six animals per group by Image J in mice 12 weeks after TAM treatment. Arrow indicates smaller adipocytes stained by PLIN1 antibody. Scale bar = 100 μm. *$P < 0.05$, **$P < 0.005$.

other organs, such as liver and heart (Fig. 1B). This was the earliest stage that we could consistently detect Bscl2 deletion in mature adipose tissues after TAM treatment. Western blot confirmed the specific deletion of Bscl2 in eWAT (Fig. 1C). Fat mass was not reduced 12 days after TAM-induced deletion, but 12 weeks after TAM administration Ad-mKO mice exhibited a 54% reduction in eWAT mass and a 45% reduction in subcutaneous WAT (sWAT) mass as compared with Ctrl mice (Fig. 1D and Fig. 1E, respectively), which resulted in an overall 40% reduction in total adiposity (Fig. 1F) and a slight 2.7% increase in lean mass (Fig. 1G). Histological analysis demonstrated an unusual pattern of adipocyte size changes in eWAT of Ad-mKO mice evidenced by increased proportions of both smaller and larger adipocytes (Fig. 1H, I), which was confirmed by immunofluorescent staining of PLIN1 (Fig. 1I). Similar findings were observed in sWAT (Fig. 1H). These data indicate that deletion of Bscl2 in mature adipocytes of adult animals regulates adiposity and adipocyte size while promoting a lean phenotype.

Bscl2 Ad-mKO mice are resistant to diet-induced obesity and dyslipidemia, but are susceptible to fatty liver and insulin resistance on a HFD

Ad-mKO mice maintained similar body weight as Ctrl mice on normal CD (**Table 1**), but gained less weight when fed with a HFD for 10 weeks starting from 12 days after TAM administration, resulting in ~70% reduction in combined WAT depot weight compared with Ctrl mice (**Fig. 2A–C**). Fasting plasma glucose and cholesterol levels were comparable between Ctrl and Ad-mKO mice on CD and HFD (Table 1). However, fasting plasma TG, NEFA, and glycerol levels were significantly lower in Ad-mKO mice on both CD and HFD, as compared with Ctrl mice on the corresponding diets (Table 1). Liver weight and TG content in Ctrl and Ad-mKO mice on CD were similar;

TABLE 1. Plasma parameters in Ctrl and Ad-mKO mice on CD and HFD

	CD		HFD	
	Ctrl (n = 6)	Ad-mKO (n = 7)	Ctrl (n = 6)	Ad-mKO (n = 6)
BW (g)	30.2 ± 0.94	30.18 ± 0.7	42.1 ± 1.4	35.4 ± 1.4[b]
Glucose (mg/dl)	144 ± 20	166 ± 20	221 ± 9	190 ± 15
TG (mg/dl)	33.5 ± 2.9	23 ± 3[a]	40.6 ± 3.6	28.2 ± 1.8[a]
Total cholesterol (mg/dl)	116 ± 22	119 ± 14	175 ± 16	195 ± 21
NEFA (mM)	0.49 ± 0.02	0.34 ± 0.05[a]	0.64 ± 0.04	0.53 ± 0.03
Glycerol (mg/dl)	28.5 ± 4	13.6 ± 1.6[a]	32 ± 3	16 ± 2[b]
Insulin (ng/ml)	0.96 ± 0.08	1.06 ± 0.14	8.1 ± 1.4	15.1 ± 3.5[a]

Male mice (8–10 weeks old) were treated with TAM for five consecutive days by gavage. Twelve days after TAM administration, mice were either maintained on CD or fed with HFD for up to 10 weeks. Plasma was collected from mice fasted for 4 h for the indicated assays. Data are presented as mean ± SE. BW, body weight.

[a] $P < 0.05$ between the Ctrl and *Ad-mKO* mice.

[b] $P < 0.005$ between the Ctrl and *Ad-mKO* mice.

however, Ad-mKO mice on HFD exhibited a 2-fold increase in liver weight (Fig. 2D) and ~130% elevation in liver TG content compared with Ctrl mice, suggesting hepatomegaly and steatosis (Fig. 2E, F). In contrast, there was no increase in skeletal muscle TG content in Ad-mKO mice on either CD or HFD, as compared with Ctrl mice (supplementary Fig. 1A). Fasting serum insulin levels were similar in both groups of mice on CD, but insulin levels

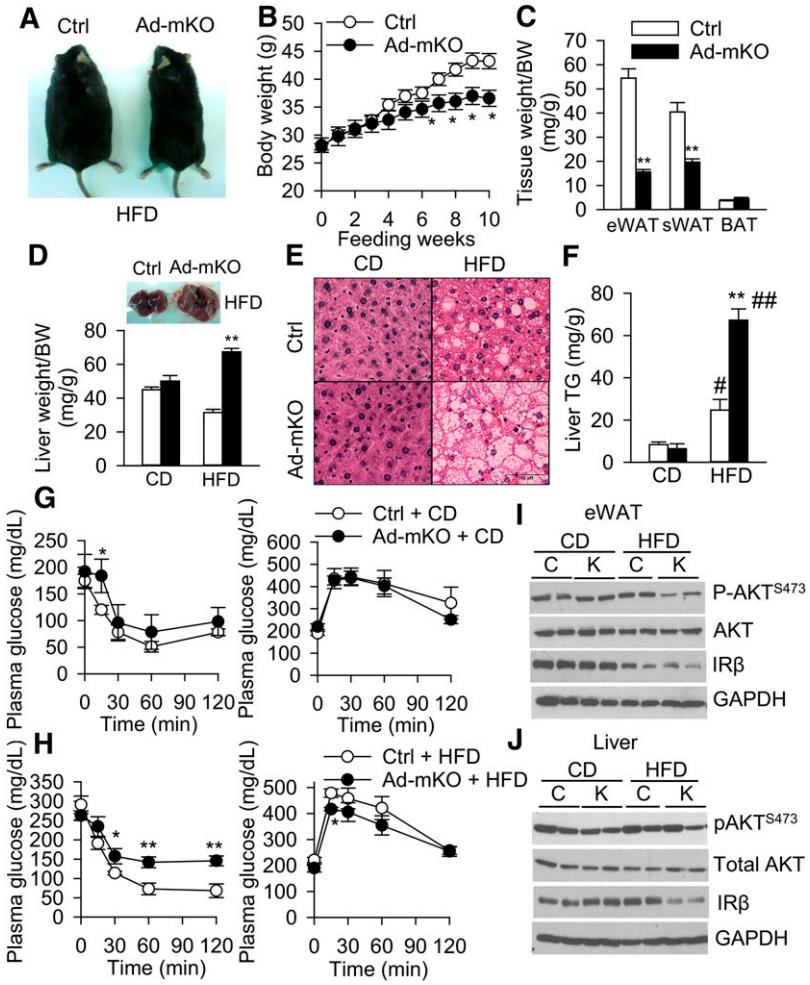

Fig. 2. Ad-mKO mice are protected from HFD-induced obesity, but are susceptible to hepatic steatosis and insulin resistance . A–C: Whole body images (A), growth curves (B), and fat tissue mass (C) in Ctrl and Ad-mKO mice fed with HFD for 10 weeks. D: Liver weight as normalized to body weight (BW). E: Liver H&E staining. Scale bar = 100 μm. F: Liver TG content in Ctrl and Ad-mKO mice on CD and HFD. G, H: Insulin tolerance test (left) and glucose tolerance test (right) on mice fed with CD (G) and HFD (H) after 6 h fast (n = 6–8 per group). I, J: Basal insulin signaling in eWAT (I) and liver (J) of Ctrl (C) and Ad-mKO (K) mice on CD and HFD after a 4 h fast. Representative Western blots from two different cohorts (n = 4 total). $*P < 0.05$, $**P < 0.005$ versus Ctrl mice on the same diet. $\#P < 0.05$, $\#\#P < 0.005$ versus CD.

were elevated in HFD-fed Ad-mKO mice, indicating insulin resistance (Table 1). Indeed, insulin sensitivity was significantly impaired in HFD-fed Ad-mKO mice (Fig. 2G, H, left panels). However, Ad-mKO mice maintained normal glucose tolerance on HFD (Fig. 2G, H, right panels) despite minimal differences in plasma insulin levels in response to glucose administration (supplementary Fig. 1B). Basal AKT phosphorylation (S473) in eWAT (Fig. 2I) and IRβ protein expression in liver (Fig. 2J) were reduced in Ad-mKO mice as compared with Ctrl mice on HFD. Basal Akt phosphorylation (S473) and IRβ protein expression in skeletal muscle were similar in both groups of mice on CD or HFD (supplementary Fig. 1C). These data suggest that eWAT and liver are the primary tissues that render HFD-fed Ad-mKO mice insulin resistant.

Acquired loss of Bscl2 in adult mature adipocytes induces browning and fatty acid oxidation

To investigate the molecular basis whereby Bscl2 deletion induces fat loss, we carried out next-generation RNA sequencing in eWAT from Ctrl and Ad-mKO mice 12 days after TAM administration. This enabled us to identify early changes in gene expression patterns induced by Bscl2 deletion, prior to the development of potentially confounding metabolic perturbations. A total of 21,976 gene transcripts were identified, and 207 genes exhibited greater than 2-fold changes in expression ($1 < \log2 < -1$, adjusted P value < 0.05) (supplementary Table 1, n = 3 pooled from nine animals). An additional 1,008 genes were differentially expressed to a lesser degree (adjusted P value < 0.05, supplementary Excel file). Genetic pathway analysis of the top 200 genes mapped to the GO biological processes linked to lipid metabolism, including fatty acid oxidation, cholesterol, sterol, and phosphatidylcholine metabolism (**Table 2**). The main transcriptional fingerprints that were substantially altered in eWAT by acquired loss of Bscl2 are shown in **Fig. 3A**. Specifically, RNA-sequencing (RNA-seq) identified >2-fold upregulated expression of genes associated with browning (*Ucp1*, *Fabp3*, *Cidea*, *Elovl3*, *Cox8b*, *Fgf21*, and *Nnat*), β-oxidation (*Cpt1β* and *Pdk4*), and mitochondrial oxidative phosphorylation (Chchd10 and Cyb5br1) following deletion of Bscl2 in mature adipocytes (Fig. 3A). Additionally, deletion of Bscl2 upregulated genes involved in sterol and cholesterol metabolism (*Insig1*, *Fdps*, and *Mvd*), phospholipid metabolism (*Pla2g2e*), glycerol phosphorylation (*Gyk*), and lipoprotein uptake (*Ldlr*). We confirmed these changes by RT-PCR in eWAT from mice 12 days after Bscl2 deletion (Fig. 3B). Immunohistochemistry and Western blotting confirmed increased UCP1 protein expression in eWAT of Ad-mKO mice 12 days after TAM administration (Fig. 3D). Meanwhile, the expression of two other important fatty acid oxidation genes [*Pparα* and *Acadl* (*Lcad*)] was consistently upregulated in eWAT of Ad-mKO mice (supplementary Excel file; Fig. 3C). In contrast, the expression of general adipocyte marker genes, including *Pparγ2*, *ap2*, and *C/ebpα*, was not altered (Fig. 3C), while leptin, a WAT marker gene (39), was downregulated (Fig. 3C). Interestingly, *Agpat2*, an enzyme governing the conversion of lysophosphatidic acid (LPA) to phosphatidic acid (PA) (40, 41), was the only TG synthesis pathway gene that was induced in eWAT 12 days after Bscl2 deletion (supplementary Excel file; Fig. 3C). By 12 weeks, the Ad-mKO mice only exhibited 34% deletion of Bscl2 [as compared with 93% deletion at 12 days (Fig. 1B)] in eWAT, but induction of browning and β-oxidation genes was largely sustained (supplementary Fig. 2A). Expression of *Pref1*, a preadipocyte marker gene (42), was substantially downregulated, while expression of

TABLE 2. Functional classification of biological processes by GOEAST [PMID: 18487275]

GO Identification	Term	Level	Log Odds-Ratio	*P*
GO:0019752	Carboxylic acid metabolic process	6	2.26	2.27E-07
GO:0032787	Monocarboxylic acid metabolic process	7	2.64	5.72E-06
GO:0006631	Fatty acid metabolic process	8	2.79	4.40E-05
GO:0019217	Regulation of fatty acid metabolic process	6	3.75	0.002402
GO:0046470	Phosphatidylcholine metabolic process	8	4.46	0.01085
GO:0009062	Fatty acid catabolic process	9	3.78	0.010955
GO:0042304	Regulation of fatty acid biosynthetic process	7	4.29	0.015209
GO:0006695	Cholesterol biosynthetic process	7	4.29	0.015209
GO:0045833	Negative regulation of lipid metabolic process	6	3.64	0.015215
GO:0008203	Cholesterol metabolic process	6	3.12	0.018173
GO:0072329	Monocarboxylic acid catabolic process	8	3.48	0.022193
GO:0006635	Fatty acid β-oxidation	10	4.00	0.027045
GO:0016126	Sterol biosynthetic process	6	4.00	0.027045
GO:0019318	Hexose metabolic process	6	2.69	0.027395
GO:0046395	Carboxylic acid catabolic process	7	2.68	0.02781
GO:0046890	Regulation of lipid biosynthetic process	6	2.96	0.029911
GO:0007169	Transmembrane receptor protein tyrosine kinase signaling pathway	7	2.23	0.031379
GO:0006656	Phosphatidylcholine biosynthetic process	9	4.82	0.032319
GO:0015908	Fatty acid transport	10	3.72	0.047506
GO:0043066	Negative regulation of apoptotic process	7	1.60	0.049827

Levels 6–10 are shown. The top 200 most differentially expressed genes were selected, and the mouse genome was chosen as background in the analysis. Results with adjusted $P < 0.05$ and Log odds-ratio >1 are listed in the order of P value. Log odds-ratio indicates the relative abundance of this GO term compared with a random situation. Log odds-ratio = 1 means that this GO term is twice as abundant in the listed genes in comparison with the random situation.

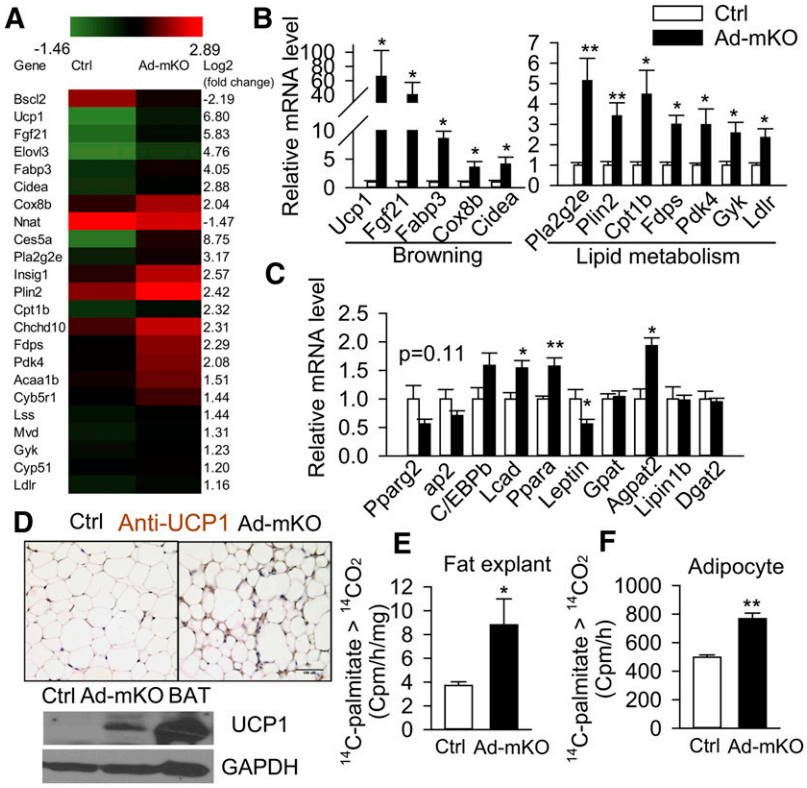

Fig. 3. Acquired loss of Bscl2 in adult adipose tissue induces browning and fatty acid oxidation. A: Heat map from RNA sequencing (three repeats pooled from nine animals per group). B, C: RT-PCR analysis of browning and lipid metabolism-related genes in eWAT 12 days after TAM treatment (n = 6 per group). D: Representative images of immunohistochemical staining (brown stain) and Western blotting for UCP1 in eWAT of Ctrl and Ad-mKO mice 12 days after TAM treatment (n = 4 each). Ctrl BAT lysate was included as positive control. Scale bar = 100 μm. E, F: Fatty acid oxidation in eWAT fat explants (n = 4 in duplicates) (E) and isolated adipocytes (1.5×10^{-5} cells per sample pooled from four animals per group) (F) based on conversion of ^{14}C-palmitate to $^{14}CO_2$. *$P < 0.05$; **$P < 0.005$.

Agpat2 and, to a lesser extent, the de novo lipogenic gene, *Scd1*, was upregulated at this time point (supplementary Fig. 2A). Increased expression of browning genes was also observed in sWAT after Bscl2 deletion, as confirmed by RT-PCR (supplementary Fig. 2B) and UCP1 staining (supplementary Fig. 2C); these changes were not sustained, however, at the 12 week time point (supplementary Fig. 2B). In line with increased expression of fatty acid oxidation genes, the production of $^{14}CO_2$ from 1-^{14}C-palmitic acid was increased >2-fold in eWAT fat explants (Fig. 3E) and 1.5-fold in isolated adipocytes (Fig. 3F) from Ad-mKO mice, as compared with Ctrl mice. These data suggest that beige adipocyte function is induced by Bscl2 deletion in WAT.

Bscl2 deletion in mature adipocytes triggers PKA-mediated lipolysis and TG breakdown

The increased fatty acid oxidation in eWAT of Ad-mKO mice prompted us to analyze whether Bscl2 deletion in mature adipocytes induces TG breakdown. Lipolysis assays performed in fat explants and isolated adipocytes from eWAT demonstrated increased release of NEFA and glycerol in Ad-mKO mice compared with Ctrl mice 12 days after TAM administration (**Fig. 4A** and Fig. 4B, respectively), suggesting that Bscl2 deletion induces lipolysis in mature WAT. PKA-mediated substrate phosphorylation (detected by antibody against phospho-PKA substrate) and HSL phosphorylation were upregulated in eWAT of Ad-mKO mice, while expression of ATGL and HSL, the two major lipases in eWAT, was unaltered. Expression of PLIN2, a PPARα targeted LD protein (43), was markedly upregulated at both the mRNA (Fig. 3A, B) and protein levels (Fig. 4C). By 12 weeks after TAM administration, changes in PKA-mediated HSL phosphorylation had largely disappeared, whereas PLIN2 protein expression remained higher in WAT of Ad-mKO mice (supplementary Fig. 3A).

Expression of M1 and M2 macrophage marker genes was unchanged 12 days after Bscl2 deletion, but was slightly upregulated after 12 weeks (supplementary Fig. 4A); immunohistochemical staining for F4/80 confirmed increased macrophage infiltration in eWAT of Ad-mKO mice (supplementary Fig. 4B). The eWAT of Ad-mKO mice also exhibited marked upregulation of ER stress marker proteins, including BIP and PDI, indicating that Bscl2 deletion induces ER stress in mature WAT (supplementary Fig. 4C). Expectedly, the eWAT of Ad-mKO mice had lower DNA content, as compared with Ctrl mice, 12 weeks after TAM administration, consistent with reduced total cell numbers in the smaller fat pads of Ad-mKO mice (supplementary Fig. 4D). Together, these data support

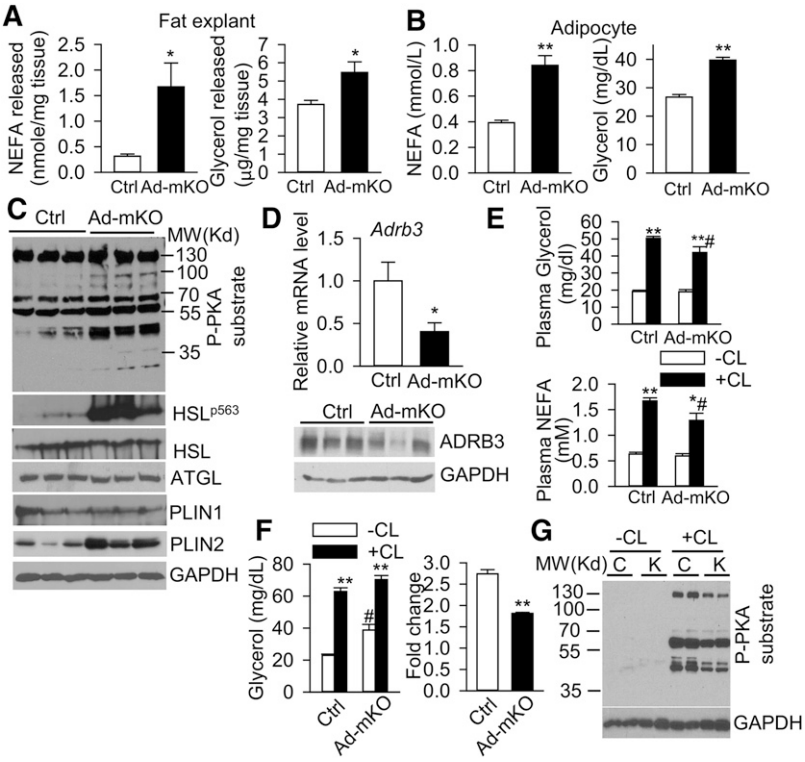

Fig. 4. Acquired loss of Bscl2 in adult adipose tissue induces basal PKA-mediated lipolysis but downregulates β3-AR signaling. A, B: NEFA and glycerol released from fat explants as normalized to tissue weight (n = 4 in duplicates) (A) and isolated adipocytes (1.5×10^5 cells per sample pooled from four animals) (B) from eWAT of Ctrl and Ad-mKO mice. C: Western blot in eWAT of Ctrl and Ad-mKO mice (n = 3). D: mRNA and protein expression of Adrb3 in eWAT of Ctrl and Ad-mKO mice (n = 6). E: Plasma NEFA and glycerol in vehicle without CL (−CL) and CL316,243 with CL (+CL) injected Ctrl and Ad-mKO mice (n = 6 per group). F: Vehicle-stimulated (−CL) and CL316,243-stimulated (+CL) glycerol release (fold change) in isolated adipocytes (1.5×10^5 cells per sample pooled from at least four Ctrl and Ad-mKO mice). Experiments in (A–F) were performed in mice 12 days after TAM injection. G: PKA-mediated phosphorylation in eWAT of 4 h-fasted Ctrl (C) and Ad-mKO (K) mice (12 weeks after TAM injection) with vehicle (−CL) and CL316,243 (+CL) stimulation for 10 min. *$P < 0.05$, **$P < 0.005$ versus Ctrl on the same treatment. #$P < 0.05$ versus –CL within same genotype.

a role for Bscl2 in regulating mature adipose tissue lipolysis and adipose depot cell content.

Acquired loss of Bscl2 in adult mature adipocytes downregulates ADRB3

Unexpectedly, RNA sequencing demonstrated that Bscl2 deletion in mature adipocytes reduced mRNA expression of *Adrb3*, a major G protein-coupled AR that regulates adipocyte lipolysis in rodents (27) (supplementary Excel file). Indeed, expression (mRNA and protein) of ADRB3 was downregulated by 50% (Fig. 4D) and remained depressed 12 weeks after Bscl2 deletion in eWAT from Ad-mKO mice (supplementary Fig. 5A). Moreover, Bscl2 deletion in Ad-mKO mice attenuated lipolytic responses to CL312,643, a specific ADRB3 agonist, as evidenced by reduced changes in circulating NEFA and glycerol levels following CL316,243 administration (Fig. 4E). The impaired CL316,243-mediated NEFA and glycerol release was further exacerbated in Ad-mKO mice 12 weeks after TAM administration (supplementary Fig. 5B), likely due to both downregulation of ADRB3 and the diminished fat mass in these mice. Plasma levels of NE were comparable between the two genotypes (supplementary Fig. 5C), suggesting that changes in ADRB3 expression in WAT were not secondary to alterations in global sympathetic tone. CL316,243-stimulated glycerol release was attenuated by >50% in isolated adipocytes from eWAT of Ad-mKO mice compared with Ctrl mice 12 days after TAM administration (Fig. 4F), confirming functional impairment of ADRB3. Basal lipolysis was minimally elevated, but responses to CL316,243 were unchanged in isolated adipocytes from eWAT of Ad-mKO mice 12 weeks after TAM administration (supplementary Fig. 5D), potentially due to diminished Bscl2 deletion efficiency at this later time point (40% in contrast to 97% 12 days after TAM injection) (supplementary Fig. 5E). Nevertheless, CL316,243-stimulated PKA substrate phosphorylation was attenuated in eWAT from Ad-mKO mice (Fig. 4G). Together, our findings are consistent with enhanced basal PKA-mediated lipolysis concomitant with a paradoxical reduction of ADRB3-stimulated lipolysis following deletion of Bscl2 in mature WAT.

Bscl2 deletion in mature adipocytes regulates whole-body energy homeostasis

We next measured indirect calorimetry in Ctrl and Ad-mKO mice 3 weeks after TAM administration, at which time body mass and composition were similar among the two groups of mice to eliminate confounding variables. Surprisingly, Ad-mKO mice fed with CD had lower food intake [expressed per mouse (**Fig. 5A**) or normalized to body weight (supplementary Fig. 6A)] during both light and dark phases, totaling a 12% reduction in caloric consumption. There was no difference in the activity levels between the two genotypes (supplementary Fig. 6B). The reduced food intake in Ad-mKO mice was independent of leptin, as plasma leptin levels were reduced in Ad-mKO mice 12 days after TAM administration and remained low (Fig. 5H), consistent with reduced leptin gene expression in eWAT of Ad-mKO mice (Fig. 3C). Oxygen consumption [expressed per mouse (Fig. 5B)] was similar in Ctrl and Ad-mKO mice, and total energy expenditure over 24 h did not differ between the two genotypes (Fig. 5C). The respiratory exchange ratio (RER), however, was lower in the dark phase in Ad-mKO mice (Fig. 5D), consistent with increased fatty acid oxidation in adipose tissues of these animals (Fig. 3E, F). These metabolic changes in Ad-mKO mice largely disappeared 12 weeks after TAM administration (Fig. 5E–G). We also measured energy expenditure in mice in response to acute NE stimulation. Heat production was attenuated (Fig. 5I), while RER (Fig. 5J) was higher after NE administration in Ad-mKO mice as compared with Ctrl mice, consistent with impaired β-adrenergic-mediated lipolysis and fatty acid oxidation. Taken together, these data suggest that targeted Bscl2 deletion in mature adipose tissue induces a leptin-independent reduction in food intake and a mild increase in energy expenditure in the face of blunted β-adrenergic-stimulated lipolysis. On balance, these effects contribute to fat loss in Ad-mKO mice.

Bscl2 deletion activates brown adipocyte lipolysis and β-oxidation without perturbing adaptive thermogenesis

We next examined whether deletion of Bscl2 in mature brown adipocytes also regulates BAT lipolysis and function. Interestingly, Ad-mKO mice demonstrated a transient increase in BAT mass at 4 weeks, which remained comparable 12 weeks after TAM administration (**Fig. 6A**). The LDs in BAT of Ad-mKO mice predominately appeared unilocular and intercalated with both small and large LDs (Fig. 6B). Despite the alterations in LDs in BAT of Ad-mKO mice, TG content was similar to Ctrl mice (Fig. 6C). However, as was observed in eWAT, PKA-mediated HSL phosphorylation was moderately increased in BAT of

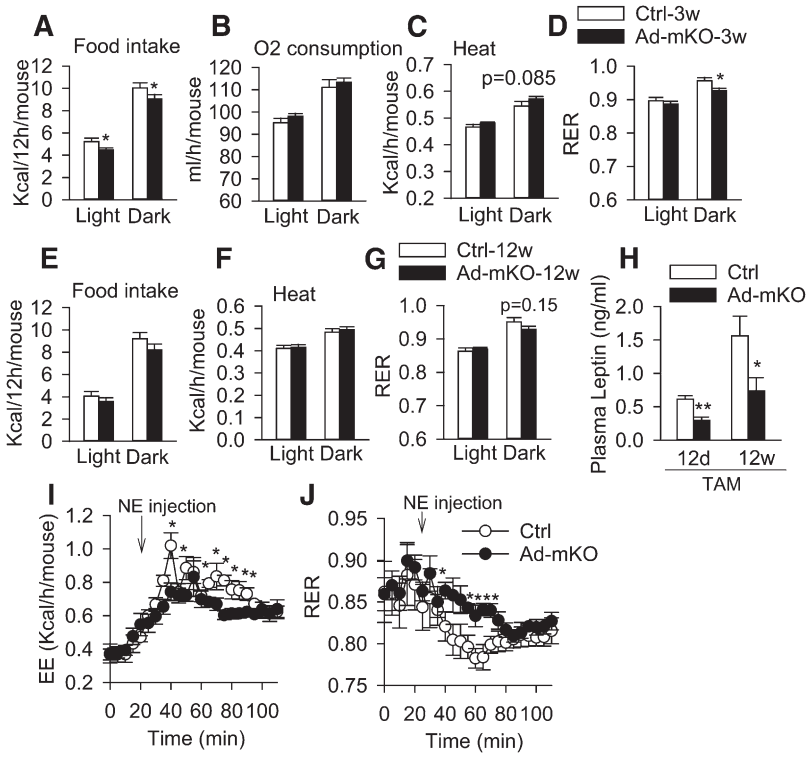

Fig. 5. Bscl2 deletion in mature adipocytes regulates food intake and energy expenditure. Food intake (A), O_2 consumption (B), heat production (C), and RER (D) in Ctrl and Ad-mKO mice 3 weeks (3w) after TAM-induced Bscl2 deletion (n = 8 per group). Food intake (E), heat production (F), and RER (G) in Ctrl and Ad-mKO mice 12 weeks after TAM treatment (n = 6). H. Plasma leptin levels in 4 h-fasted Ctrl and Ad-mKO mice 12 days (12d) and 12 weeks (12w) after TAM injection (n = 6–8). Energy expenditure (EE) (I) and RER (J) in response to NE stimulation in Ctrl and Ad-mKO mice 12 weeks after TAM injection (n = 6–7). $^{*}P < 0.05$, $^{**}P < 0.005$.

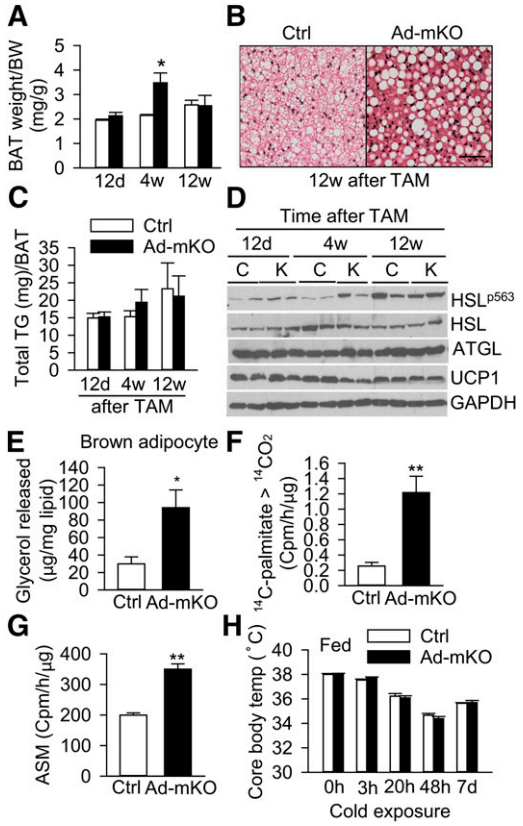

Fig. 6. Bscl2 deletion in mature brown adipocytes activates lipolysis and β-oxidation. A: BAT weight normalized to body weight (BW) in Ctrl and Ad-mKO mice 12 days (12d), 4 weeks (4w), and 12 weeks (12w) after TAM-induced Bscl2 deletion (n = 6 per group). B: H&E staining of BAT from Ctrl and Ad-mKO mice 12 weeks after TAM. C, D: TG content normalized to BAT weight (n = 6/group) (C) and Western blot (D) of BAT in Ctrl and Ad-mKO mice fasted for 4 h at different stages as indicated. E: Lipolysis in isolated brown adipocytes (normalized to lipid content). F, G: Fatty acid oxidation rate of BAT homogenates based on conversion of ^{14}C-palmitic acid to $^{14}CO_2$ (F) and acid soluble metabolites (ASM) (G) (n = 6 per group). H: Core body temperature measured before and after cold exposure of fed Ctrl and Ad-mKO mice for the indicated hours and days (d) (n = 6–8 per group). Panels (B) and (E–H) were performed on mice 12 weeks after TAM treatment. $^{*}P < 0.05$; $^{**}P < 0.005$.

Ad-mKO mice at early stages (12 days to 4 weeks), which normalized by 12 weeks after Bscl2 deletion (Fig. 6D). Isolated brown adipocytes from Ad-mKO mice also exhibited increased basal lipolysis (Fig. 6E), and BAT homogenates from these mice converted more ^{14}C-palmitate to $^{14}CO_2$ (Fig. 6F) and acid soluble metabolite (Fig. 6G), suggesting enhanced fatty acid oxidation capacity. The expression of brown adipocyte marker and β-oxidation genes was similar in the two groups of mice, but there was ∼30% reduction in *Adrb3* gene expression 12 weeks after Bscl2 deletion (supplementary Fig. 7A, B). Bscl2 deletion in mature adipose tissue was not associated with changes in brown adipocyte recruitment (assessed by DNA content per brown fat pad) or mitochondrial biogenesis (assessed by mitochondrial copy number per nucleus) (supplementary Fig. 7C, D). Also, UCP1 protein expression in skeletal muscle was similar in the two groups of mice (supplementary Fig. 7E). Despite the alterations in BAT and browning of WAT following deletion of Bscl2, rectal temperature was comparable between the two cohorts under ambient temperature (21°C), and body temperature unexpectedly remained similar after cold exposure in the presence of food for up to 7 days (Fig. 6H), suggesting preserved adaptive thermogenesis in Ad-mKO mice.

Thermoneutrality enhances body mass loss in Ad-mKO mice

Ambient temperature conditions (i.e., 21°C) impose a chronic thermal stress on mice which activates β-adrenergic signaling, adipocyte lipolysis, and fat metabolism (44). To determine whether reduced ADRB3 expression in Ad-mKO mice counter-regulates the browning-induced fat loss and energy expenditure at ambient temperature, we examined the effect of Bscl2 ablation under conditions whereby sympathetic activation was abrogated (i.e., at thermoneutrality, ∼30°C for mice) (44). We acclimated adult animals at 30°C for 1 week before administering TAM to induce Bscl2 deletion and then kept the mice at this temperature. By 12 weeks, the Ad-mKO mice weighed less than the Ctrl mice (**Fig. 7A**). Loss of eWAT and sWAT mass was greater as compared with that observed at 21°C (67% at 30°C vs. 54% at 21°C for eWAT; 57% at 30°C vs. 45% at 21°C for sWAT) (Fig. 7B). In contrast, the weights of BAT and liver were increased in Ad-mKO mice under these conditions, suggesting that the primary effect of Bscl2 deletion under thermoneutral conditions is white fat loss. Histology revealed multi-locular LDs in both the eWAT and sWAT, but enlarged WAT-like unilocular LDs in BAT of Ad-mKO mice (Fig. 7C). Moreover, PKA-mediated HSL phosphorylation and PLIN2 protein expression were upregulated in eWAT of Ad-mKO mice at thermoneutrality 12 weeks after Bscl2 deletion (Fig. 7D). Not surprisingly, eWAT from Ad-mKO mice housed at 30°C exhibited different gene expression profiles compared with Ctrl mice, with increased expression of browning genes and genes involved in β-oxidation, and slightly decreased expression of *Adrb3* (Fig. 7E). These data suggest that the impact of Bscl2 ablation on metabolism and fat mass is more pronounced when animals are housed at thermoneutrality and sympathetic activity is low.

DISCUSSION

Utilizing a novel mouse model in which Bscl2 is inducibly deleted in adipocytes of adult animals, we have characterized the impact of acquired deficiency of Bscl2 in mature adipose tissues (as opposed to the impact of embryonic Bscl2 gene deletion on adipocyte differentiation/adipose tissue development). Our data strongly suggest that loss of Bscl2 upregulates cAMP/PKA-mediated lipolysis, browning, and lipid oxidation to induce fat loss, which is partially offset by blunted adipose tissue β-adrenergic signaling through reduced ADRB3 receptor expression (**Fig. 8**). These changes highlight an important role for Bscl2 in regulating adipose tissue lipolysis, metabolism, and whole-body energy balance in adult animals.

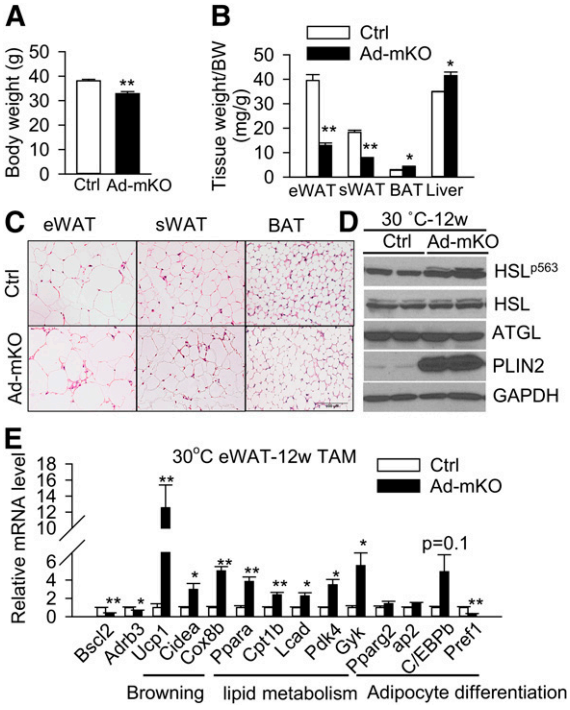

Fig. 7. Thermoneutrality (30°C) enhances weight loss and lipid mobilization in Ad-mKO mice. A, B: Body weight (BW) (A) and tissue weight (B) as normalized to body weight. C: H&E staining of fat tissues. Scale bar = 100 μm. D, E: Western blot (D) and RT-PCR analyses (E) of eWAT (4 h fast). All data were collected from mice at thermoneutrality 12 weeks after TAM injection (n = 6 per group). Representative Western blot is shown. $*P < 0.05$, $**P < 0.005$.

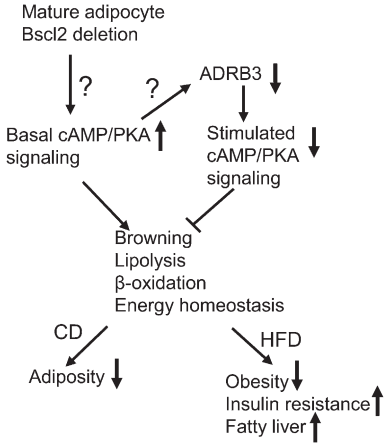

Fig. 8. Proposed mechanisms whereby loss of Bscl2 regulates function of mature adipocytes. Acquired loss of Bscl2 in mature adipocytes activates basal cAMP/PKA-mediated lipolysis, browning, and lipid catabolism in adipose tissues, but paradoxically downregulates ADRB3 expression. Despite reducing adrenergic-stimulated lipolysis, deletion of Bscl2 in mature adipocytes promotes a lean phenotype in mice fed a CD and protects against HFD-induced obesity, but not insulin resistance and hepatic steatosis. How Bscl2 regulates basal cAMP/PKA signaling and causes downregulation of ADRB3 remains unknown.

Global gene expression profiling and biochemical data suggest that Bscl2 regulates cAMP/PKA signaling in WAT and BAT, and that its loss promotes lipolysis and TG breakdown in vivo. Notably, the changes in gene expression profile in eWAT consequent to acquired Bscl2 deletion largely resemble those observed with β3-AR agonist stimulation and cold exposure, including lipolysis and browning (45–48), acute repression of leptin (49–52), increased Gyk expression, and cholesterol metabolism (53), inflammation, and ER stress (54–56). Browning may result from the direct conversion of mature white adipocytes into beige cells, given that Bscl2 deletion is directed toward adiponectin-expressing cells in our model. The enhanced lipolysis resulting from Bscl2 deletion yields ligands that can activate PPARα (57), which in turn increases fatty acid oxidation and oxidative phosphorylation. Increased fatty acid oxidation was also reported in *Drosophila dSeipin*$^{-/-}$ fat body (18) and in residual eWAT of global Bscl2-deficient mice (58). PLIN2 is typically not expressed by mature adipocytes (59), but was detected during hormone-stimulated lipolysis (60) and in adipose tissues of mice with elevated lipolysis (35, 53, 61). Thus, upregulated PLIN2 in Ad-mKO adipose tissues is consistent with increased lipolysis, corroborating our findings in differentiating Bscl2$^{-/-}$ mouse embryonic fibroblasts and in residual adipose tissues from *Bscl2*$^{-/-}$ mice (10). Overall, these data suggest that besides inducing cAMP/PKA-mediated lipolysis to inhibit adipocyte differentiation, Bscl2 deletion also stimulates lipolysis, browning, and lipid oxidation in mature adipocytes, resulting in attenuated adiposity and protection from diet-induced obesity.

Interestingly, our findings reveal countervailing effects of Bscl2 deletion on lipolysis: namely, reduced adipocyte expression of ADRB3 and β-adrenergic-stimulated lipolysis, which opposed the increased basal lipolysis and fat loss in animals maintained at ambient temperature. Increased cAMP/PKA signaling has been reported in some, but not all, studies to downregulate ADRB3 in WAT (54, 62, 63). Reduced ADRB3 expression in Bscl2-deleted adipose tissues suggests an intrinsic negative crosstalk between Bscl2 and β3-AR signaling, although the mechanism remains to be determined. Blunted ADRB3-dependent signaling opposed the effect of browning to increase energy expenditure at ambient temperature (21°C), and in response to adaptive thermogenesis, in Ad-mKO mice. Collectively, these phenomena emphasize a complex role for Bscl2 in modulating sympathetic activation of adipocytes and whole-body energy balance that depend, in part, upon environmental conditions.

Targeted Bscl2 deletion in mature adipocytes unexpectedly attenuated food intake, in contrast to the hyperphagic effects of embryonic global Bscl2 gene deletion (10–12). While the hyperphagia in *Bscl2*$^{-/-}$ mice can be attributed to leptin deficiency caused by an absence of adipose tissue, the lower plasma level of leptin in Ad-mKO mice suggests a leptin-independent mechanism for reduced food intake in Ad-mKO mice. One potential explanation is upregulated expression of Gdf15, a newly-identified anorexigenic adipokine (64). While the mRNA expression of Gdf15 was significantly increased in Ad-mKO mice (supplementary Table 1), whether circulating Gdf15 levels are sufficient to negatively regulate food intake remains to be

established. Importantly, reductions in caloric intake in Ad-mKO mice are not sufficient to fully account for the magnitude of fat loss. Hence, a combination of increased energy expenditure consequent to browning of WAT, concurrent with reduced food intake, contributes to the lean phenotype and obesity resistance in Ad-mKO mice.

Our studies provide new molecular insight into the role of Bscl2 in mediating adipocyte lipid metabolism. First, deletion of Bscl2 in adipose tissues of Ad-mKO mice was associated with upregulated expression of several genes involved in phospholipid metabolism, including *Pla2g2e*, choline kinase β (*Chkb*), sphingosine-1-phosphate lyase 1 (*Sgpl1*), and *Agpat2* (supplementary Excel file; Fig. 3). The upregulation of *Agpat2* in adipose tissues of Ad-mKO mice is particularly interesting, as mutations in human *AGPAT2* cause type 1 BSCL (65). Importantly, Agpat2 overexpression increased PA levels in 3T3-L1 adipocytes (41), and elevated PA levels were observed in eWAT of ASKO mice (19). Human BSCL2 also forms a complex with human AGPAT2 and LPIN1 in vitro (20, 21), but whether these proteins interact with each other in vivo is unknown. Second, increased lipolysis could alter phospholipid metabolism in Ad-mKO mice, as TG hydrolysis provides substrate for the CDP-choline pathway of phospholipid synthesis (66, 67). Finally, altered phospholipid metabolism, known to regulate LD size (68), might also contribute to the unusual LD morphology observed in adipocytes of Ad-mKO mice.

Our findings in Ad-mKO mice reinforce the role of Bscl2 in regulating function of mature adipocytes, as reported in ASKO mice (19). These two mouse models share many metabolic features, including insulin resistance, adipose inflammation, ER stress, and protection against obesity. However, in contrast to ASKO mice, Ad-mKO mice develop hepatic steatosis only on a HFD, exhibit less adipose tissue macrophage infiltration, and remain glucose tolerant. The lack of an intrinsic role for Bscl2 in regulating liver fatty acid oxidation, as demonstrated in mice with liver-specific Bscl2 deletion (69), suggests that steatosis in Ad-mKO mice fed a HFD results from increased circulating fatty acids consequent to dysfunctional WAT. The absence of glucose intolerance despite insulin resistance in Ad-mKO mice is potentially explained by upregulated expression of genes involved in the hexose metabolic pathway in eWAT of Ad-mKO mice (supplementary Excel file; Table 2), leading to increased glucose metabolism. Indeed, activation of cAMP/PKA signaling in WAT and BAT has been shown to be associated with increased glucose metabolism (70–72). The extent to which this functions to preserve glucose tolerance in Ad-mKO mice is unclear and will require further investigation. It is important to point out that FABP4-Cre mediates the continuous deletion of *Bscl2* in differentiating and mature adipocytes, leading to a more lipodystrophic phenotype in ASKO mice as compared with Ad-mKO mice. Moreover, in Ad-mKO mice, TAM-induced deletion of *Bscl2* in mature adipose tissue appears to trigger the turnover of Bscl2-deficient adipocytes and the formation of new Bscl2-expressing adipocytes from preadipocytes, as suggested by time-dependent reductions in Bscl2 deletion efficiency and *Pref*1 expression. This adipocyte turnover progressively attenuates the impact of Bscl2 gene deletion in Ad-mKO mice and results in a lean but not lipodystrophic phenotype.

The exact mechanisms whereby Bscl2 regulates cAMP/PKA-mediated lipolysis remain unknown. Bscl2 was reported to interact with SERCA to regulate calcium signaling in the fat body of *Drosophila* (18). However, a direct link between calcium signaling and PKA-mediated lipolysis in mammalian adipocytes has not been reported. As Bscl2 lacks homology to any proteins with known function, predicting its ultimate target is very challenging. Lack of a specific antibody that can localize the endogenous Bscl2 protein by immunofluorescent or immunochemical staining is also a significant limitation. The close genomic vicinity of *Bscl2* to *Gng3* (32), and the presence of a unique CAAX prenylation motif on Bscl2 resembling a G protein γ subunit (33), suggest that Bscl2 may coordinate G protein signaling, although this hypothesis remains to be tested.

In summary, we demonstrate that adipocyte-specific Bscl2 deletion induces lipolysis and browning in mature adipose tissues but paradoxically downregulates ADRB3, thus exerting a complex effect on whole-body energy homeostasis. Our data further highlight Bscl2 as a regulator of lipolytic pathways that have important relevance to lipid metabolism, body composition, and obesity, independent of its role in adipocyte differentiation and adipose tissue development.

The authors wish to thank Vanderbilt Mouse Metabolic Phenotyping Center (DK059637) for performing indirect calorimetry, body composition analysis, and plasma epinephrine measurement.

REFERENCES

1. Agarwal, A. K., R. I. Barnes, and A. Garg. 2004. Genetic basis of congenital generalized lipodystrophy. *Int. J. Obes. Relat. Metab. Disord.* **28:** 336–339.
2. Berardinelli, W. 1954. An undiagnosed endocrinometabolic syndrome: report of 2 cases. *J. Clin. Endocrinol. Metab.* **14:** 193–204.
3. Seip, M., and O. Trygstad. 1996. Generalized lipodystrophy, congenital and acquired (lipoatrophy). *Acta Paediatr. Suppl.* **413:** 2–28.
4. Garg, A., R. Wilson, R. Barnes, E. Arioglu, Z. Zaidi, F. Gurakan, N. Kocak, S. O'Rahilly, S. I. Taylor, S. B. Patel, et al. 1999. A gene for congenital generalized lipodystrophy maps to human chromosome 9q34. *J. Clin. Endocrinol. Metab.* **84:** 3390–3394.
5. Hayashi, Y. K., C. Matsuda, M. Ogawa, K. Goto, K. Tominaga, S. Mitsuhashi, Y. E. Park, I. Nonaka, N. Hino-Fukuyo, K. Haginoya, et al. 2009. Human PTRF mutations cause secondary deficiency of caveolins resulting in muscular dystrophy with generalized lipodystrophy. *J. Clin. Invest.* **119:** 2623–2633.
6. Kim, C. A., M. Delepine, E. Boutet, H. El Mourabit, S. Le Lay, M. Meier, M. Nemani, E. Bridel, C. C. Leite, D. R. Bertola, et al. 2008. Association of a homozygous nonsense caveolin-1 mutation with Berardinelli-Seip congenital lipodystrophy. *J. Clin. Endocrinol. Metab.* **93:** 1129–1134.
7. Magré, J., M. Delépine, E. Khallouf, T. Gedde-Dahl, Jr., L. Van Maldergem, E. Sobel, J. Papp, M. Meier, A. Mégarbané, A. Bachy, et al. 2001. Identification of the gene altered in Berardinelli-Seip congenital lipodystrophy on chromosome 11q13. *Nat. Genet.* **28:** 365–370.

8. Agarwal, A. K., and A. Garg. 2003. Congenital generalized lipodystrophy: significance of triglyceride biosynthetic pathways. *Trends Endocrinol. Metab.* **14:** 214–221.
9. Chen, W., V. K. Yechoor, B. H. Chang, M. V. Li, K. L. March, and L. Chan. 2009. The human lipodystrophy gene product Berardinelli-Seip congenital lipodystrophy 2/seipin plays a key role in adipocyte differentiation. *Endocrinology.* **150:** 4552–4561.
10. Chen, W., B. Chang, P. Saha, S. M. Hartig, L. Li, V. T. Reddy, Y. Yang, V. Yechoor, M. A. Mancini, and L. Chan. 2012. Berardinelli-Seip congenital lipodystrophy 2/seipin is a cell-autonomous regulator of lipolysis essential for adipocyte differentiation. *Mol. Cell. Biol.* **32:** 1099–1111.
11. Cui, X., Y. Wang, Y. Tang, Y. Liu, L. Zhao, J. Deng, G. Xu, X. Peng, S. Ju, G. Liu, et al. 2011. Seipin ablation in mice results in severe generalized lipodystrophy. *Hum. Mol. Genet.* **20:** 3022–3030.
12. Prieur, X., L. Dollet, M. Takahashi, M. Nemani, B. Pillot, C. Le May, C. Mounier, H. Takigawa-Imamura, D. Zelenika, F. Matsuda, et al. 2013. Thiazolidinediones partially reverse the metabolic disturbances observed in Bscl2/seipin-deficient mice. *Diabetologia.* **56:** 1813–1825.
13. Ebihara, C., K. Ebihara, M. Aizawa-Abe, T. Mashimo, T. Tomita, M. Zhao, V. Gumbilai, T. Kusakabe, Y. Yamamoto, D. Aotani, et al. 2015. Seipin is necessary for normal brain development and spermatogenesis in addition to adipogenesis. *Hum. Mol. Genet.* **24:** 4238–4249.
14. Fei, W., G. Shui, B. Gaeta, X. Du, L. Kuerschner, P. Li, A. J. Brown, M. R. Wenk, R. G. Parton, and H. Yang. 2008. Fld1p, a functional homologue of human seipin, regulates the size of lipid droplets in yeast. *J. Cell Biol.* **180:** 473–482.
15. Szymanski, K. M., D. Binns, R. Bartz, N. V. Grishin, W. P. Li, A. K. Agarwal, A. Garg, R. G. Anderson, and J. M. Goodman. 2007. The lipodystrophy protein seipin is found at endoplasmic reticulum lipid droplet junctions and is important for droplet morphology. *Proc. Natl. Acad. Sci. USA.* **104:** 20890–20895.
16. Fei, W., G. Shui, Y. Zhang, N. Krahmer, C. Ferguson, T. S. Kapterian, R. C. Lin, I. W. Dawes, A. J. Brown, P. Li, et al. 2011. A role for phosphatidic acid in the formation of "supersized" lipid droplets. *PLoS Genet.* **7:** e1002201.
17. Wolinski, H., D. Kolb, S. Hermann, R. I. Koning, and S. D. Kohlwein. 2011. A role for seipin in lipid droplet dynamics and inheritance in yeast. *J. Cell Sci.* **124:** 3894–3904.
18. Bi, J., W. Wang, Z. Liu, X. Huang, Q. Jiang, G. Liu, Y. Wang, and X. Huang. 2014. Seipin promotes adipose tissue fat storage through the ER Ca^{2+}-ATPase SERCA. *Cell Metab.* **19:** 861–871.
19. Liu, L., Q. Jiang, X. Wang, Y. Zhang, R. C. Lin, S. M. Lam, G. Shui, L. Zhou, P. Li, Y. Wang, et al. 2014. Adipose-specific knockout of SEIPIN/BSCL2 results in progressive lipodystrophy. *Diabetes.* **63:** 2320–2331.
20. Sim, M. F., R. J. Dennis, E. M. Aubry, N. Ramanathan, H. Sembongi, V. Saudek, D. Ito, S. O'Rahilly, S. Siniossoglou, and J. J. Rochford. 2012. The human lipodystrophy protein seipin is an ER membrane adaptor for the adipogenic PA phosphatase lipin 1. *Mol. Metab.* **2:** 38–46.
21. Talukder, M. M., M. F. Sim, S. O'Rahilly, J. M. Edwardson, and J. J. Rochford. 2015. Seipin oligomers can interact directly with AGPAT2 and lipin 1, physically scaffolding critical regulators of adipogenesis. *Mol. Metab.* **4:** 199–209.
22. Harms, M., and P. Seale. 2013. Brown and beige fat: development, function and therapeutic potential. *Nat. Med.* **19:** 1252–1263.
23. Langin, D. 2010. Recruitment of brown fat and conversion of white into brown adipocytes: strategies to fight the metabolic complications of obesity? *Biochim. Biophys. Acta.* **1801:** 372–376.
24. Bartelt, A., and J. Heeren. 2012. The holy grail of metabolic disease: brown adipose tissue. *Curr. Opin. Lipidol.* **23:** 190–195.
25. Giacobino, J. P. 1995. Beta 3-adrenoceptor: an update. *Eur. J. Endocrinol.* **132:** 377–385.
26. Bachman, E. S., H. Dhillon, C. Y. Zhang, S. Cinti, A. C. Bianco, B. K. Kobilka, and B. B. Lowell. 2002. betaAR signaling required for diet-induced thermogenesis and obesity resistance. *Science.* **297:** 843–845.
27. Grujic, D., V. S. Susulic, M. E. Harper, J. Himms-Hagen, B. A. Cunningham, B. E. Corkey, and B. B. Lowell. 1997. Beta3-adrenergic receptors on white and brown adipocytes mediate beta3-selective agonist-induced effects on energy expenditure, insulin secretion, and food intake. A study using transgenic and gene knockout mice. *J. Biol. Chem.* **272:** 17686–17693.
28. Hu, B., and L. L. Jennings. 2003. Orally bioavailable beta 3-adrenergic receptor agonists as potential therapeutic agents for obesity and type-II diabetes. *Prog. Med. Chem.* **41:** 167–194.
29. Weyer, C., P. A. Tataranni, S. Snitker, E. Danforth, Jr., and E. Ravussin. 1998. Increase in insulin action and fat oxidation after treatment with CL 316,243, a highly selective beta3-adrenoceptor agonist in humans. *Diabetes.* **47:** 1555–1561.
30. Cannon, B., and J. Nedergaard. 2004. Brown adipose tissue: function and physiological significance. *Physiol. Rev.* **84:** 277–359.
31. Sassmann, A., S. Offermanns, and N. Wettschureck. 2010. Tamoxifen-inducible Cre-mediated recombination in adipocytes. *Genesis.* **48:** 618–625.
32. Bligh, E. G., and W. J. Dyer. 1959. A rapid method of total lipid extraction and purification. *Can. J. Biochem. Physiol.* **37:** 911–917.
33. Samuel, V. T., Z. X. Liu, X. Qu, B. D. Elder, S. Bilz, D. Befroy, A. J. Romanelli, and G. I. Shulman. 2004. Mechanism of hepatic insulin resistance in non-alcoholic fatty liver disease. *J. Biol. Chem.* **279:** 32345–32353.
34. Xue, Y., N. Petrovic, R. Cao, O. Larsson, S. Lim, S. Chen, H. M. Feldmann, Z. Liang, Z. Zhu, J. Nedergaard, et al. 2009. Hypoxia-independent angiogenesis in adipose tissues during cold acclimation. *Cell Metab.* **9:** 99–109.
35. Liew, C. W., J. Boucher, J. K. Cheong, C. Vernochet, H. J. Koh, C. Mallol, K. Townsend, D. Langin, D. Kawamori, J. Hu, et al. 2013. Ablation of TRIP-Br2, a regulator of fat lipolysis, thermogenesis and oxidative metabolism, prevents diet-induced obesity and insulin resistance. *Nat. Med.* **19:** 217–226.
36. Kim, K. H., Y. T. Jeong, H. Oh, S. H. Kim, J. M. Cho, Y. N. Kim, S. S. Kim, H. Kim do, K. Y. Hur, H. K. Kim, et al. 2013. Autophagy deficiency leads to protection from obesity and insulin resistance by inducing Fgf21 as a mitokine. *Nat. Med.* **19:** 83–92.
37. Hirschey, M. D., T. Shimazu, E. Goetzman, E. Jing, B. Schwer, D. B. Lombard, C. A. Grueter, C. Harris, S. Biddinger, O. R. Ilkayeva, et al. 2010. SIRT3 regulates mitochondrial fatty-acid oxidation by reversible enzyme deacetylation. *Nature.* **464:** 121–125.
38. Chang, B. H., L. Li, A. Paul, S. Taniguchi, V. Nannegari, W. C. Heird, and L. Chan. 2006. Protection against fatty liver but normal adipogenesis in mice lacking adipose differentiation-related protein. *Mol. Cell. Biol.* **26:** 1063–1076.
39. Mori, M. A., T. Thomou, J. Boucher, K. Y. Lee, S. Lallukka, J. K. Kim, M. Torriani, H. Yki-Jarvinen, S. K. Grinspoon, A. M. Cypess, et al. 2014. Altered miRNA processing disrupts brown/white adipocyte determination and associates with lipodystrophy. *J. Clin. Invest.* **124:** 3339–3351.
40. Cortés, V. A., D. E. Curtis, S. Sukumaran, X. Shao, V. Parameswara, S. Rashid, A. R. Smith, J. Ren, V. Esser, R. E. Hammer, et al. 2009. Molecular mechanisms of hepatic steatosis and insulin resistance in the AGPAT2-deficient mouse model of congenital generalized lipodystrophy. *Cell Metab.* **9:** 165–176.
41. Subauste, A. R., A. K. Das, X. Li, B. G. Elliott, C. Evans, M. El Azzouny, M. Treutelaar, E. Oral, T. Leff, and C. F. Burant. 2012. Alterations in lipid signaling underlie lipodystrophy secondary to AGPAT2 mutations. *Diabetes.* **61:** 2922–2931.
42. Sul, H. S. 2009. Pref-1: Role in adipogenesis and mesenchymal cell fate. *Mol. Endocrinol.* **23:** 1717–1725.
43. Dalen, K. T., S. M. Ulven, B. M. Arntsen, K. Solaas, and H. I. Nebb. 2006. PPARalpha activators and fasting induce the expression of adipose differentiation-related protein in liver. *J. Lipid Res.* **47:** 931–943.
44. Golozoubova, V., H. Gullberg, A. Matthias, B. Cannon, B. Vennstrom, and J. Nedergaard. 2004. Depressed thermogenesis but competent brown adipose tissue recruitment in mice devoid of all hormone-binding thyroid hormone receptors. *Mol. Endocrinol.* **18:** 384–401.
45. Cousin, B., S. Cinti, M. Morroni, S. Raimbault, D. Ricquier, L. Penicaud, and L. Casteilla. 1992. Occurrence of brown adipocytes in rat white adipose tissue: molecular and morphological characterization. *J. Cell Sci.* **103:** 931–942.
46. Loncar, D., B. A. Afzelius, and B. Cannon. 1988. Epididymal white adipose tissue after cold stress in rats. I. Nonmitochondrial changes. *J. Ultrastruct. Mol. Struct. Res.* **101:** 109–122.
47. Loncar, D., L. Bedrica, J. Mayer, B. Cannon, J. Nedergaard, B. A. Afzelius, and A. Svajger. 1986. The effect of intermittent cold treatment on the adipose tissue of the cat. Apparent transformation from white to brown adipose tissue. *J. Ultrastruct. Mol. Struct. Res.* **97:** 119–129.
48. Young, P., J. R. Arch, and M. Ashwell. 1984. Brown adipose tissue in the parametrial fat pad of the mouse. *FEBS Lett.* **167:** 10–14.

49. Mantzoros, C. S., D. Qu, R. C. Frederich, V. S. Susulic, B. B. Lowell, E. Maratos-Flier, and J. S. Flier. 1996. Activation of beta(3) adrenergic receptors suppresses leptin expression and mediates a leptin-independent inhibition of food intake in mice. *Diabetes.* **45:** 909–914.
50. Gettys, T. W., P. J. Harkness, and P. M. Watson. 1996. The beta 3-adrenergic receptor inhibits insulin-stimulated leptin secretion from isolated rat adipocytes. *Endocrinology.* **137:** 4054–4057.
51. Puerta, M., M. Abelenda, M. Rocha, and P. Trayhurn. 2002. Effect of acute cold exposure on the expression of the adiponectin, resistin and leptin genes in rat white and brown adipose tissues. *Horm. Metab. Res.* **34:** 629–634.
52. Trayhurn, P., J. S. Duncan, and D. V. Rayner. 1995. Acute cold-induced suppression of ob (obese) gene expression in white adipose tissue of mice: mediation by the sympathetic system. *Biochem. J.* **311:** 729–733.
53. Dong, M., X. Yang, S. Lim, Z. Cao, J. Honek, H. Lu, C. Zhang, T. Seki, K. Hosaka, E. Wahlberg, et al. 2013. Cold exposure promotes atherosclerotic plaque growth and instability via UCP1-dependent lipolysis. *Cell Metab.* **18:** 118–129.
54. Granneman, J. G., P. Li, Z. Zhu, and Y. Lu. 2005. Metabolic and cellular plasticity in white adipose tissue I: effects of beta3-adrenergic receptor activation. *Am. J. Physiol. Endocrinol. Metab.* **289:** E608–E616.
55. Li, P., Z. Zhu, Y. Lu, and J. G. Granneman. 2005. Metabolic and cellular plasticity in white adipose tissue II: role of peroxisome proliferator-activated receptor-alpha. *Am. J. Physiol. Endocrinol. Metab.* **289:** E617–E626.
56. Mottillo, E. P., X. J. Shen, and J. G. Granneman. 2010. beta3-adrenergic receptor induction of adipocyte inflammation requires lipolytic activation of stress kinases p38 and JNK. *Biochim. Biophys. Acta.* **1801:** 1048–1055.
57. Mottillo, E. P., A. E. Bloch, T. Leff, and J. G. Granneman. 2012. Lipolytic products activate peroxisome proliferator-activated receptor (PPAR) alpha and delta in brown adipocytes to match fatty acid oxidation with supply. *J. Biol. Chem.* **287:** 25038–25048.
58. Chen, W., H. Zhou, S. Liu, C. J. Fhaner, B. C. Gross, T. A. Lydic, and G. E. Reid. 2013. Altered lipid metabolism in residual white adipose tissues of bscl2 deficient mice. *PLoS One.* **8:** e82526.
59. Brasaemle, D. L., T. Barber, N. E. Wolins, G. Serrero, E. J. Blanchette-Mackie, and C. Londos. 1997. Adipose differentiation-related protein is an ubiquitously expressed lipid storage droplet-associated protein. *J. Lipid Res.* **38:** 2249–2263.
60. Gross, D. N., H. Miyoshi, T. Hosaka, H. H. Zhang, E. C. Pino, S. Souza, M. Obin, A. S. Greenberg, and P. F. Pilch. 2006. Dynamics of lipid droplet-associated proteins during hormonally stimulated lipolysis in engineered adipocytes: stabilization and lipid droplet binding of adipocyte differentiation-related protein/adipophilin. *Mol. Endocrinol.* **20:** 459–466.
61. Nishino, N., Y. Tamori, S. Tateya, T. Kawaguchi, T. Shibakusa, W. Mizunoya, K. Inoue, R. Kitazawa, S. Kitazawa, Y. Matsuki, et al. 2008. FSP27 contributes to efficient energy storage in murine white adipocytes by promoting the formation of unilocular lipid droplets. *J. Clin. Invest.* **118:** 2808–2821.
62. Jaworski, K., M. Ahmadian, R. E. Duncan, E. Sarkadi-Nagy, K. A. Varady, M. K. Hellerstein, H. Y. Lee, V. T. Samuel, G. I. Shulman, K. H. Kim, et al. 2009. AdPLA ablation increases lipolysis and prevents obesity induced by high-fat feeding or leptin deficiency. *Nat. Med.* **15:** 159–168.
63. Klaus, S., P. Muzzin, J. P. Revelli, M. A. Cawthorne, J. P. Giacobino, and D. Ricquier. 1995. Control of beta 3-adrenergic receptor gene expression in brown adipocytes in culture. *Mol. Cell. Endocrinol.* **109:** 189–195.
64. Tsai, V. W., L. Macia, H. Johnen, T. Kuffner, R. Manadhar, S. B. Jorgensen, K. K. Lee-Ng, H. P. Zhang, L. Wu, C. P. Marquis, et al. 2013. TGF-b superfamily cytokine MIC-1/GDF15 is a physiological appetite and body weight regulator. *PLoS One.* **8:** e55174.
65. Agarwal, A. K., E. Arioglu, S. De Almeida, N. Akkoc, S. I. Taylor, A. M. Bowcock, R. I. Barnes, and A. Garg. 2002. AGPAT2 is mutated in congenital generalized lipodystrophy linked to chromosome 9q34. *Nat. Genet.* **31:** 21–23.
66. Carman, G. M., and S. A. Henry. 1999. Phospholipid biosynthesis in the yeast Saccharomyces cerevisiae and interrelationship with other metabolic processes. *Prog. Lipid Res.* **38:** 361–399.
67. Dowd, S. R., M. E. Bier, and J. L. Patton-Vogt. 2001. Turnover of phosphatidylcholine in Saccharomyces cerevisiae. The role of the CDP-choline pathway. *J. Biol. Chem.* **276:** 3756–3763.
68. Fei, W., H. Li, G. Shui, T. S. Kapterian, C. Bielby, X. Du, A. J. Brown, P. Li, M. R. Wenk, P. Liu, et al. 2011. Molecular characterization of seipin and its mutants: implications for seipin in triacylglycerol synthesis. *J. Lipid Res.* **52:** 2136–2147.
69. Chen, W., H. Zhou, P. Saha, L. Li, and L. Chan. 2014. Molecular mechanisms underlying fasting modulated liver insulin sensitivity and metabolism in male lipodystrophic Bscl2/Seipin-deficient mice. *Endocrinology.* **155:** 4215–4225.
70. Chernogubova, E., B. Cannon, and T. Bengtsson. 2004. Norepinephrine increases glucose transport in brown adipocytes via beta3-adrenoceptors through a cAMP, PKA, and PI3-kinase-dependent pathway stimulating conventional and novel PKCs. *Endocrinology.* **145:** 269–280.
71. Cooney, G. J., I. D. Caterson, and E. A. Newsholme. 1985. The effect of insulin and noradrenaline on the uptake of 2-[1-14C]deoxyglucose in vivo by brown adipose tissue and other glucose-utilising tissues of the mouse. *FEBS Lett.* **188:** 257–261.
72. Liu, X., F. Perusse, and L. J. Bukowiecki. 1994. Chronic norepinephrine infusion stimulates glucose uptake in white and brown adipose tissues. *Am. J. Physiol.* **266:** R914–R920.